

Small-scale
transport structures
in the Arctic winter
2009/2010

C. Kalicinsky et al.

Small-scale transport structures in the Arctic winter 2009/2010

C. Kalicinsky¹, J.-U. Grooß², G. Günther², J. Ungermann², J. Blank², S. Höfer², L. Hoffmann³, P. Knieling¹, F. Olschewski¹, R. Spang², F. Stroh², and M. Riese²

¹Department of Physics, University of Wuppertal, Wuppertal, Germany

²Institute of Energy and Climate Research – Stratosphere (IEK-7), Research Centre Jülich GmbH, Jülich, Germany

³Jülich Supercomputing Centre, Research Centre Jülich GmbH, Jülich, Germany

Received: 6 March 2013 – Accepted: 6 April 2013 – Published: 19 April 2013

Correspondence to: C. Kalicinsky (kalicins@uni-wuppertal.de)

Published by Copernicus Publications on behalf of the European Geosciences Union.

Title Page

Abstract

Introduction

Conclusions

References

Tables

Figures

⏪

⏩

◀

▶

Back

Close

Full Screen / Esc

Printer-friendly Version

Interactive Discussion

Abstract

The CRISTA-NF (Cryogenic Infrared Spectrometers and Telescope for the Atmosphere – New Frontiers) instrument is an airborne infrared limb sounder operated aboard the Russian research aircraft M55-Geophysica. The instrument successfully participated in a large Arctic aircraft campaign within the RECONCILE (Reconciliation of essential process parameters for an enhanced predictability of Arctic stratospheric ozone loss and its climate interactions) project from January to March 2010 in Kiruna, Sweden.

This paper concentrates on the measurements during one flight of the campaign, which took place on 2 March in the vicinity of the polar vortex. We present two-dimensional cross-sections of volume mixing ratios for the trace gases CFC-11, O₃, and ClONO₂ with an unprecedented vertical resolution of about 500 to 600 m for a large part of the observed altitude range and a dense horizontal sampling along flight direction of ≈ 15 km. The trace gas distributions show several structures like the polar vortex and filaments composed of air masses of different origin.

The situation during the analysed flight is simulated by the chemistry and transport model CLaMS (Chemical Lagrangian Model of the Stratosphere) and compared with the measurements to assess the performance of the model with respect to advection, mixing, and the chemistry in the polar vortex. These comparisons confirm the capability of CLaMS to reproduce even very small-scale structures in the atmosphere. Based on the good agreement between simulation and observation, we use a model concept utilising artificial tracers to further analyse the CRISTA-NF observations in terms of air mass origin. A characteristic of the Arctic winter 2009/10 was a sudden stratospheric warming in early December that led to a split of the polar vortex. The vortex re-established at the end of December. Our passive tracer simulations suggest that large parts of the re-established vortex consisted to about 45 % of high- and mid-latitude air.

ACPD

13, 10463–10498, 2013

Small-scale transport structures in the Arctic winter 2009/2010

C. Kalicinsky et al.

Title Page

Abstract

Introduction

Conclusions

References

Tables

Figures

⏪

⏩

◀

▶

Back

Close

Full Screen / Esc

Printer-friendly Version

Interactive Discussion

1 Introduction

The upper troposphere/lower stratosphere (UTLS) region plays an important role in the climate system (e.g. IPCC, 2007; Riese et al., 2012). Changes in the chemical composition of this region result in particularly large changes in radiative forcing of the atmosphere. Therefore, quantifying the chemical composition of this region and the underlying processes represents a crucial task. During winter and spring, the composition of the lower Arctic stratosphere is strongly influenced by mixing of polar and mid-latitude air masses, a process that is associated with the occurrence of fine trace gas structures and filaments. These structures can be considered as part of a scale cascade from synoptic-scale streamers over elongated filaments down to small-scale three-dimensional turbulence. While horizontal exchange of tropical and polar air masses in form of synoptic-scale streamers has been observed by global infrared limb-observations by the Cryogenic Infrared Spectrometers and Telescopes for the Atmosphere (CRISTA) instrument (e.g. Riese et al., 1999, 2002), in-situ observations on high-flying research aircraft provided a wealth of information on small-scale mixing processes (e.g. Hoor et al., 2002; Konopka et al., 2004). In this paper, we present observations of filamentary trace gas structures made by the airborne Cryogenic Infrared Spectrometers and Telescope for the Atmosphere – New Frontiers (CRISTA-NF) instrument. These observations fill the gap between global satellite observations and airborne in-situ measurements in terms of spatial resolution and coverage.

CRISTA-NF is an infrared limb sounder, which utilises the center telescope and spectrometer gratings of the satellite instrument CRISTA (e.g. Offermann et al., 1999; Grossmann et al., 2002). The instrument measures thermal emissions of trace gases (4 to 15 μm) with a high vertical sampling (≈ 250 m) and dense horizontal sampling along flight track (≈ 15 km). The employed retrieval scheme allows for deriving profiles of selected trace gases with a very high vertical resolution (up to about 400 m; Ungermann et al., 2012). CRISTA-NF is operated aboard the high-flying Russian research aircraft M55-Geophysica which offers a maximum flight altitude of about 20 km and, therefore,

Small-scale transport structures in the Arctic winter 2009/2010

C. Kalicinsky et al.

Title Page

Abstract

Introduction

Conclusions

References

Tables

Figures



Back

Close

Full Screen / Esc

Printer-friendly Version

Interactive Discussion



is an ideal platform for limb measurements of UTLS composition. The instrument was successfully flown on board M55-Geophysica during the tropical aircraft campaigns SCOUT-O3 (e.g. Hoffmann et al., 2009; Spang et al., 2008) and AMMA-SCOUT-O3 (e.g. Weigel et al., 2012).

In this paper, we discuss observations of polar vortex air masses and fine filamentary structures based on two-dimensional distributions of the trace gases CFC-11, O₃, and ClONO₂ with unprecedented vertical resolution for atmospheric limb sounding (Unger-
mann et al., 2012). The observations were made during a M55-Geophysica flight from Spitsbergen to Kiruna/Sweden on 2 March 2010 in the framework of the European RECONCILE project (Reconciliation of essential process parameters for an enhanced predictability of Arctic stratospheric ozone loss and its climate interactions; von Hobe et al., 2012). During this flight, M55-Geophysica encountered an interesting meteorological situation, where a large number of small-scale structures (incl. pronounced filaments) was observed in the spatial distributions of CFC-11, ozone, chlorine nitrate, and other trace gases. We analyse these observations based on ozone-CFC-11-relations and simulations with the Chemical Lagrangian Model of the Stratosphere (CLaMS; e.g. McKenna et al., 2002b,a), which includes a passive tracer concept for air mass origin analyses (Günther et al., 2008).

The CRISTA-NF instrument is briefly introduced in Sect. 2. Section 3 gives an overview on the CLaMS simulations used for our analyses. The meteorological situation and the CRISTA-NF observations are described in Sects. 4 and 5. In Sect. 6, we show that the passive tracer concept of CLaMS provides further insight into the origin of the trace gas structures observed by CRISTA-NF. Furthermore, we use the passive tracer concept to assess the effects of a sudden stratospheric warming (SSW) that occurred in early December 2009 (associated with a vortex split) on the re-established polar vortex (end of December 2009). A short summary and some conclusions are given in Sect. 7.

Small-scale transport structures in the Arctic winter 2009/2010

C. Kalicinsky et al.

Title Page

Abstract

Introduction

Conclusions

References

Tables

Figures



Back

Close

Full Screen / Esc

Printer-friendly Version

Interactive Discussion

2 CRISTA-NF observations

CRISTA-NF measures thermal emissions of several atmospheric trace gases (e.g. CFC-11, O₃, ClONO₂, HNO₃) in the spectral range from 4 to 15 μm and in the altitude range from flight altitude (up to 20 km) down to 5 km. Kullmann et al. (2004) give a detailed insight into the design of the cryostat and the optical system of CRISTA-NF. The calibration procedure and improvements concerning the data processing for the RECONCILE aircraft campaign are described by Schroeder et al. (2009) and Ungermann et al. (2012), respectively.

The viewing direction of the instrument is perpendicular to the flight direction to the right side of the aircraft. A Herschel telescope with a tiltable mirror scans the atmosphere with a vertical sampling of about 250 m. The incoming radiance is spectrally dispersed by the two Ebert-Fastie (e.g. Fastie, 1991) grating spectrometers with different spectral resolution of $\lambda/\Delta\lambda \sim 1000$ and 500, respectively, and finally measured by semiconductor detectors (Si : Ga) that are operated at temperatures of about 13 K. These low temperatures allow for a measurement speed of ≈ 1.2 s per spectrum coupled with a good signal to noise ratio. A complete altitude scan consisting of 60 spectra can be performed within ≈ 70 s. Based on the speed of the aircraft this fast measurement speed leads to a horizontal sampling along flight direction of about 15 km.

The fine vertical and horizontal sampling combined with a comparably small vertical field of view (FOV) of 3 arc min (≈ 300 m at 10 km tangent height, Spang et al., 2008) provides the basis for the retrieval of two-dimensional trace gas distributions with high spatial resolution (Ungermann et al., 2012).

To obtain the retrieval results shown in Sect. 5 we use a setup of 13 integrated micro windows (IMW) in the spectral range from 775 cm⁻¹ to 865 cm⁻¹, which is covered by the CRISTA-NF low resolution spectrometer detector channel number 6 (LRS 6). The trace gas profiles are derived by means of the Juelich RAPid Spectral Simulation Code version 2 (JURASSIC2; e.g. Ungermann et al., 2010, 2013), a further development of JURASSIC, which was successfully used to analyse measurements from various

ACPD

13, 10463–10498, 2013

Small-scale
transport structures
in the Arctic winter
2009/2010

C. Kalicinsky et al.

Title Page

Abstract

Introduction

Conclusions

References

Tables

Figures

⏪

⏩

◀

▶

Back

Close

Full Screen / Esc

Printer-friendly Version

Interactive Discussion

**Small-scale
transport structures
in the Arctic winter
2009/2010**

C. Kalicinsky et al.

Title Page

Abstract

Introduction

Conclusions

References

Tables

Figures

◀

▶

◀

▶

Back

Close

Full Screen / Esc

Printer-friendly Version

Interactive Discussion

satellites and airborne limb-emission measurements (e.g. Hoffmann et al., 2008; Hoffmann and Alexander, 2009; Weigel et al., 2012). The main targets of the retrieval are CFC-11, O₃, ClONO₂, HNO₃, H₂O, and CCl₄. In addition, aerosol, temperature, PAN, CFC-113, and HCFC-22 are retrieved from the measurements as secondary targets.

The list of the used IMWs and the corresponding retrieval targets is displayed in Table 1. A full error analysis is performed regarding all non-retrieved gases, instrument errors, forward model errors, spectroscopic line uncertainties and the smoothing error. The combined errors of trace gas volume mixing ratios for CFC-11 are typically between 15 and 20 pptv and the errors for ClONO₂ and ozone in average about 15%. Remarkable is the unprecedented vertical resolution of 400 m to 500 m for CFC-11 in the altitude range from flight altitude down to approximately 12 km. The vertical resolution in this altitude range is about 500 m to 600 m and 500 m to 1 km for O₃ and ClONO₂, respectively. The retrieval technique and validation against measurements by other instruments is described in detail by Weigel et al. (2010) and Ungermann et al. (2012), respectively. The derivation of the trace gas cross-sections was since improved by means of cross-sections retrievals to further reduce the effect of stochastic errors such as a remaining line-of-sight uncertainty (Ungermann, 2013).

3 CLaMS simulations

The model used in the following sections for comparison and further analyses is the Chemical Lagrangian Model of the Stratosphere (CLaMS). It was first developed as a two-dimensional model on isentropic surfaces (McKenna et al., 2002b) and later on extended to three dimensions by application of cross-isentropic transport (Konopka et al., 2004). The introduction of the hybrid vertical coordinate ζ (equal to the potential temperature in the stratosphere and parallel to the pressure isolines in the troposphere) expanded the model to the tropopause region and the troposphere (Konopka et al., 2007).

**Small-scale
transport structures
in the Arctic winter
2009/2010**C. Kalicinsky et al.

[Title Page](#)[Abstract](#)[Introduction](#)[Conclusions](#)[References](#)[Tables](#)[Figures](#)[⏪](#)[⏩](#)[◀](#)[▶](#)[Back](#)[Close](#)[Full Screen / Esc](#)[Printer-friendly Version](#)[Interactive Discussion](#)

CLaMS simulates an ensemble of air parcels moving along trajectories, which are calculated by means of meteorological wind fields. Each transport step consists of an advection step, in which the air parcels follow the trajectories, and a subsequent mixing step. The mixing step is realised utilising a dynamically adaptive grid. If the distance between an air parcel and one of its prior nearest neighbours falls below/exceeds a certain threshold criterion defined by the Lyapunov exponent λ_c , the two air parcels are merged and a new air parcel is inserted in between the two former ones, respectively. The characteristics of a new or merged air parcel are the mean characteristics of the two prior air parcels. The mixing strength is adjusted by the Lyapunov exponent λ_c (logarithmic expansion rate), where a smaller value induces more mixing and vice versa. A detailed description of the dynamically adaptive grid is given by McKenna et al. (2002b) and Konopka et al. (2004).

The model includes 48 chemical species and 144 chemical reactions (84 binary, 13 ternary, 36 photolysis, 11 heterogeneous), which is an update of McKenna et al. (2002a). The formation, sedimentation, and evaporation of NAT (nitric acid trihydrate) particles is realised by means of a Lagrangian sedimentation tool described by Grooß et al. (2005) to simulate de- and renitrification processes in the stratosphere.

The simulations were initialised on 1 December 2009. The atmospheric trace gases are partly initialised utilising globally distributed measurements by three satellite instruments (Microwave Limb Sounder aboard AURA satellite (AURA–MLS; Waters et al., 2006), Atmospheric Chemistry Experiment – Fourier Transform Spectrometer (ACE–FTS; Bernath et al., 2005) and Michelson Interferometer for Passive Atmospheric Sounding–ENVISAT (MIPAS–ENV; Fischer et al., 2008)) and partly using correlations between trace gases or partitioning within chemical families.

A model concept utilising artificial (passive) tracers is used to analyse air masses in terms of their origin (see, e.g. Günther et al., 2008). A whole set of these tracers, each of them representing a different type of air mass (tropics, mid-latitudes, high-latitudes, and vortex), is applied in the model. Hence, each air parcel includes four passive tracers describing the origin of the air masses. The passive tracers of an air parcel are

**Small-scale
transport structures
in the Arctic winter
2009/2010**C. Kalicinsky et al.

[Title Page](#)[Abstract](#)[Introduction](#)[Conclusions](#)[References](#)[Tables](#)[Figures](#)[⏪](#)[⏩](#)[◀](#)[▶](#)[Back](#)[Close](#)[Full Screen / Esc](#)[Printer-friendly Version](#)[Interactive Discussion](#)

initialised based on values of modified potential vorticity (mPV) of this air parcel at the initialisation date. Modified potential vorticity is a scaled form of potential vorticity (PV) to reduce the altitude dependence of PV, which is increasing with increasing altitude. Details about the description and derivation of mPV are given by Lait (1994) and Müller and Günther (2003). Table 3 summarises the mPV boundary conditions for each passive tracer. The boundaries are chosen because they roughly coincide with the boundaries between the different air mass types. For example, the boundary value of 19.8 potential vorticity units (PVU; $10^{-6} \text{ K m}^2 (\text{kg s})^{-1}$) agrees very well with the vortex edge defined by the criterion after Nash et al. (1996). In the context of this paper, the air mass type high-latitude denotes air masses in the transition region between the vortex edge and the mid-latitudes. If an air parcel fulfils one of the given conditions, the corresponding passive tracer is set to 1 and all other tracers to zero. In the model simulation these tracers are only advected and mixed. Thus, the sum of all tracers in one air parcels is always 1 and the value of each single passive tracer gives the proportion of the corresponding air mass type, whereby 1 denotes 100 %. The composition of an air parcel in terms of the passive tracers therefore reflects the composition of the air masses in terms of their origin and can be used to analyse mixing processes and to identify different air masses. We use two different initialisation dates for the passive tracers. On the one hand, the passive tracers are initialised on 1 December 2009 (identical to initialisation date of the trace gases and starting point of simulation) and, on the other hand, the passive tracers are initialised on 15 January 2010 in a second simulation to analyse the evolution of the vortex during the aircraft campaign (17 January 2010 to 10 March 2010). In the latter case only the passive tracers are initialised on 15 January, whereas everything else is identical to the simulation described above.

4 Flight path and meteorological situation

During the RECONCILE aircraft campaign 12 flights took place in the time period from 17 January to 10 March 2010. The flight (flight 11 of the campaign) discussed in this

of the polar vortex down to a potential temperature of about 350 K. Due to this fact the mPV cross-section shown in Fig. 2 is displayed in the altitude range from flight altitude down to 10.5 km (approximately 350 K potential temperature).

The polar vortex is clearly visible at the beginning of the flight indicated by a high mPV value (larger than 20 PVU; compare Table 3). The vertical extent of this area with high mPV goes from flight altitude down to about 15 km. Thus, the first part of the flight took place inside the polar vortex and the aircraft left it at about 11:15 UTC. The edge of the vortex is indicated by the steep gradient in mPV. Additionally, a second prominent structure showing high mPV values is visible at the end of the flight below 16 km. The mPV values in this structure are in the range from 16 to 20 PVU. These high values indicate most likely air masses with a high fraction of air originating from the polar vortex. Apart from these two areas with high mPV values, an area showing mPV values below 12 PVU is visible immediately below flight altitude at the end of the flight. The air masses in this area are therefore most likely of mid- or low-latitude origin.

In summary, the cross-section of modified PV shows three distinct areas: the polar vortex, a structure with a high fraction of vortex air masses and an area containing air masses probably originating from mid- or low-latitudes.

5 CRISTA-NF retrieval results

In this section we present the trace gas distributions of CFC-11, O₃, and ClONO₂ derived from CRISTA-NF measurements. Furthermore, the origin of air masses in different observed structures is analysed using ozone-CFC-11-relations.

Figure 3 displays the cross-sections of CFC-11, ClONO₂, and ozone for flight 11. The first trace gas CFC-11 is chemical inert and has a stratospheric lifetime of about 45 yr (WMO, 2007). Thus, it is well suited to analyse dynamical processes in the lower stratosphere. The latter two trace gases are mainly involved in the ozone chemistry inside the polar vortex in winter and spring. All retrieval results are displayed between flight altitude and the lowest tangent height of a valid measurement in the corresponding

Title Page

Abstract

Introduction

Conclusions

References

Tables

Figures



Back

Close

Full Screen / Esc

Printer-friendly Version

Interactive Discussion



in a region with moderate values of modified PV, indicating a different origin. The horizontal distribution of PV (not shown here) shows that the two structures are vertical cuts through filamentary structures. The two areas at the end of the flight showing low CFC-11 VMRs are hereafter denoted as lower and upper filament.

The cross-sections of ClONO₂ and O₃ (Fig. 3b and c) confirm these observations. The area identified as polar vortex shows very high ClONO₂ VMRs up to 1.5 ppbv. These high values are caused by the subsidence of the air masses inside the polar vortex and the chlorine deactivation after the cold phase of the vortex and the presence of polar stratospheric clouds. The main process after the onset of chlorine deactivation in the Arctic is the formation of ClONO₂ via the reaction of ClO and NO₂, whereas the formation of HCl (via the reaction of Cl and CH₄) is slowed down because of the typically small Cl/ClO fraction in the Arctic (e.g. Douglass et al., 1995; Santee et al., 2008). Thus, very high ClONO₂ VMRs, larger than at the beginning of the winter, are expected in early March inside the vortex and vortex air masses.

The ozone VMRs inside the polar vortex are lower or equal to the volume mixing ratios outside the vortex at comparable altitudes. These VMRs are a consequence of the ozone depletion inside the vortex. If no chemical ozone depletion would have occurred, the ozone VMRs inside the vortex would be larger than outside the vortex because of the subsidence of air masses inside the vortex and the related downward transport of ozone rich air masses from higher altitudes. This argument is valid below ≈ 475 K (flight altitude inside the vortex ≈ 450 K).

The ozone and ClONO₂ VMRs inside the two filaments at the end of the flight show large differences, although the CFC-11 volume mixing are very similar. The O₃ VMRs in the upper filament are significantly higher and the ClONO₂ VMRs significantly lower than the corresponding values in the lower filament. Therefore, only the air masses inside the lower filament show the influence of chlorine deactivation and ozone depletion. This confirms that only the lower filament contains air masses with a large fraction of vortex air.

Small-scale transport structures in the Arctic winter 2009/2010

C. Kalicinsky et al.

[Title Page](#)[Abstract](#)[Introduction](#)[Conclusions](#)[References](#)[Tables](#)[Figures](#)[⏪](#)[⏩](#)[◀](#)[▶](#)[Back](#)[Close](#)[Full Screen / Esc](#)[Printer-friendly Version](#)[Interactive Discussion](#)

**Small-scale
transport structures
in the Arctic winter
2009/2010**

C. Kalicinsky et al.

Title Page

Abstract

Introduction

Conclusions

References

Tables

Figures

⏪

⏩

◀

▶

Back

Close

Full Screen / Esc

Printer-friendly Version

Interactive Discussion



In order to analyse these differences of the air masses inside the both filaments in more detail the ozone-CFC-11-relation is used here. Fig. 4a shows a scatter-plot of CFC-11 and O_3 for the retrieved cross-section. Two characteristic curves are visible that are caused by different relationships between stratospheric trace gases in this regions (e.g. Plumb, 2007). Inside the polar vortex a relation involving ozone changes during the winter because of ozone depletion leading to an increasing difference between inside vortex air masses and outside vortex air masses (e.g. Müller et al., 2005). This can be used to differentiate between vortex and non vortex air masses in spring. By selecting air parcels stemming obviously from the vortex branch (here: CFC-11 VMRs of less than 70 pptv and O_3 VMRs of less than 2.7 ppbv) and parcels stemming from outside the vortex (here: O_3 VMRs above 2.7 ppbv or between 0.6 and 1.6 ppbv), one can determine typical correlations for vortex and non-vortex air in the given situation. For simplicities sake we use linear correlations here. These correlations can then be used to automatically identify vortex and non-vortex air. For certain parcels, no definite judgement can be made, as the correlation lines meet. Finally, the assignment of parcels can be transferred from tracer-tracer space to geo-spatial space and is shown in Fig. 4b. The lower part of the polar vortex can be identified above 15.5 km in the first half of the flight. Also the classification of the lower and upper filament at 12:30 UTC is asserted, as only the lower filament has the chemical relationship between CFC-11 and O_3 typical for vortex air. In addition, at least one further small filament of vortex air is suggested by the chemical relationship at 11:30 UTC and 14 km altitude.

6 Comparison of CRISTA-NF and CLaMS and analysis of the air mass origin

This section proceeds with the comparison of the CRISTA-NF results and simulations by CLaMS to assess the performance of the model. Additionally, the concept of passive tracers, which is capable to identify different air masses, is analysed by means of the CRISTA-NF results.

All CLaMS results are interpolated in time and space onto the CRISTA-NF retrieval grid. Thereby, two CLaMS model outputs at two different times, one before the flight start and the other after the flight end, are used. A vertical convolution of the CLaMS results with the averaging kernels of the retrieval results is omitted, since the vertical resolution of the CRISTA-NF and CLaMS results is very similar.

6.1 Comparison of trace gases

Figure 5a displays the cross-section of the CLaMS result for CFC-11. The distribution of CFC-11 is mainly determined by advection and mixing processes and therefore well suited to assess the performance of CLaMS in terms of these processes.

All main structures observed by CRISTA-NF are well reproduced by CLaMS. The polar vortex and the two observed filaments with low CFC-11 VMRs are visible in the CLaMS result, albeit the horizontal location and extent of the structures is slightly different. Even the thin layer with higher CFC-11 VMRs between the two filaments and the air masses with enhanced VMRs immediately below the flight path at the end of the flight are captured by CLaMS. Nevertheless, some small differences can be seen. For example, the small-scale structures in the vortex edge region around 11:20 UTC between 17 km and 14 km are missing in the model result. But according to the different horizontal resolution of both results (CRISTA-NF \approx 15 km; CLaMS \approx 70 km), these small differences are at least partly caused by the lower resolution of CLaMS. However, the CFC-11 cross-sections are quantitatively and qualitatively in a very good agreement, which indicates the good performance of CLaMS in terms of advection and mixing.

The cross-section of ClONO₂ is shown in Fig. 5b. The CLaMS result is in a good agreement with the CRISTA-NF retrieval result, albeit some differences inside the vortex and the vortex filament are visible. Inside the lower filament at the end of the flight the ClONO₂ VMRs of the CLaMS result are lower compared to the retrieval result. Furthermore, the vertical extent of the area with very high volume mixing ratios below flight altitude at the beginning of the flight is smaller in the CLaMS result. These differences give a hint for small deficiencies in the chlorine activation and deactivation by CLaMS.

Title Page

Abstract

Introduction

Conclusions

References

Tables

Figures



Back

Close

Full Screen / Esc

Printer-friendly Version

Interactive Discussion



Small-scale transport structures in the Arctic winter 2009/2010

C. Kalicinsky et al.

Title Page

Abstract

Introduction

Conclusions

References

Tables

Figures

⏪

⏩

◀

▶

Back

Close

Full Screen / Esc

Printer-friendly Version

Interactive Discussion



Figure 5c shows the CLaMS result for ozone. By comparison to the CRISTA-NF retrieval result, the only obvious difference is visible in the polar vortex, where the CLaMS result exhibits higher ozone VMRs. A maximum discrepancy of up to 0.4 ppmv can be seen. This difference is most likely a consequence of an underestimation of the ozone depletion by CLaMS that may be related to deficiencies in the simulated chlorine activation (see above). Comparisons between CLaMS results for HCl (not measured by CRISTA-NF) with satellite measurements by AURA-MLS and ACE-FTS in the time period from the beginning of December to end of March (not shown in this paper) confirm the assumption. Inside the polar vortex in January the HCl VMRs of CLaMS are significantly higher than those of the satellite measurements in the analysed altitude range from 400 K to 550 K. This indicates an underestimation of the chlorine activation from the reservoir species HCl, which leads to an underestimation of the ozone depletion. Since the chlorine deactivation in the Arctic at the beginning is mainly driven by the formation of ClONO₂, the observed differences for ClONO₂ are most likely a consequence of this underestimation of chlorine activation as well.

In summary, CLaMS is well suited to simulate the observed situation, especially for the tracer CFC-11. In the following, we therefore use the observed CFC-11 field together with the passive tracer concept of CLaMS to gain further insight in the origin of the observed air masses.

6.2 Air mass origin

In Sect. 5 we showed that CRISTA-NF observed the polar vortex and a vortex filament during RECONCILE flight 11 on 2 March 2010. Thus, this data-set is suitable to analyse the capability of the CLaMS passive tracers to identify different air masses. The history of the polar vortex during the whole winter is essential for the interpretation of the results for the passive tracers and the comparisons with the observations. In winter 2009/2010 the polar vortex splitted twice during two sudden stratospheric warmings. The first split occurred in December and the vortex re-established again at end of December. During this split event some mid-latitude air masses were included into the

Small-scale transport structures in the Arctic winter 2009/2010

C. Kalicinsky et al.

Title Page

Abstract

Introduction

Conclusions

References

Tables

Figures



Back

Close

Full Screen / Esc

Printer-friendly Version

Interactive Discussion

vortex. The second split took place in February and the two parts of the vortex re-joined in early March. A discussion about the evolution of the vortex is given, e.g. by Dörnbrack et al. (2012); von Hobe et al. (2012). The CRISTA-NF observations therefore took place in a part of the rejoining vortex at the beginning of March. In order to get a better comparison with these observations and to analyse the evolution of the vortex during the aircraft campaign (17 January 2010 to 10 March 2010) we use the passive tracers initialised on 15 January 2010, and, therefore, exclude the vortex split in December from the analysis. Thus, all air masses inside the vortex on 15 January, which includes also air masses transported into the vortex during December, were initialised as vortex air masses.

The cross-section of the CLaMS vortex tracer is shown in Fig. 6a for the time of observation. The vortex fraction inside the polar vortex partly exceeds 0.9 at the highest altitudes. Thus, the part of the polar vortex observed by CRISTA-NF on 2 March is comparable to the vortex on 15 January in terms of the composition as indicated by the very high values of the vortex fraction. The vortex fraction in the core of the vortex filament located at the end of the flight at 14 km is larger than 0.7. In the region of the upper filament (around 17 km at the end of the flight) the vortex tracer is very low indicating only a minor fraction of vortex air masses in this region. These results are in a very good agreement with the observations by CRISTA-NF, which showed that the lower filament with low CFC-11 VMRs is a vortex filament and the air masses in the upper filament are of different origin by means of ozone-CFC-11-relations (compare Sect. 5). Hence, by using the initialisation date of 15 January, the CLaMS vortex tracer provides a picture which is consistent to the air mass classification obtained from the CRISTA-NF measurements (compare Fig. 4b). This suggests that other passive tracers can be used to analyse the whole situation during the flight in more detail.

Figure 6b displays the cross-section for the low-latitude tracer. At the end of the flight in the region between flight altitude and 15 km the low-latitude tracer reaches values up to 0.5. The areas of high low-latitude fraction correspond to the areas showing higher CFC-11 VMRs immediately below flight altitude and between the two filaments with

**Small-scale
transport structures
in the Arctic winter
2009/2010**C. Kalicinsky et al.

[Title Page](#)[Abstract](#)[Introduction](#)[Conclusions](#)[References](#)[Tables](#)[Figures](#)[Back](#)[Close](#)[Full Screen / Esc](#)[Printer-friendly Version](#)[Interactive Discussion](#)

the flight can hardly be seen. Thus, the vortex tracer initialised on 1 December cannot provide a picture that is consistent with the CRISTA-NF observations, because of the in-mixing of air masses into the vortex in December and consequently a change in the vortex composition. However, a comparison between the passive tracers of both initialisations provide information on the amount of air masses mixed into the vortex. The difference of the passive tracers of both initialisations inside the polar vortex between 10:05 and 11:00 UTC (excluding the ascent and the vortex edge region) around flight altitude (≈ 450 K potential temperature) is illustrated in Fig. 8. The boxes show the average values of the passive tracers inside the polar vortex for both initialisation dates. Obviously, the polar vortex was very stable after 15 January, which is illustrated by the very high average value of the vortex fraction (blue) for the January initialisation of ≈ 0.90 . Hence, only very few air masses mixed into the vortex after 15 January. Thus, the large difference between the vortex fraction of both initialisation dates (≈ 0.47 for December initialisation to ≈ 0.90 for January initialisation) can be almost attributed to the in-mixing of air masses into the vortex during December and gives a reasonable estimate of the amount of air masses mixed into the vortex. These air masses account for about 45 % of the total air masses inside the re-established polar vortex at the end of December.

Since the sum of all passive tracers in one air parcel is always 1, the positive change in the vortex fraction has to be compensated by negative changes in the remaining tracers (high-latitude, mid-latitude, low-latitude). These changes are visible in Fig. 8 by a reduction of the high- and mid-latitude fractions from December to January initialisation. These reductions in relation to the change in the vortex fraction or the ratio of the average values of the high- and mid-latitude fraction for the December initialisation (about 70 : 30) give an estimate of the contributions of both air mass types to the air masses mixed into the vortex. Hence, high-latitude air masses contributed most to the air masses mixed into the vortex (about 70 %) and mid-latitude air masses were the second important contributor (about 30 %). The contribution of low-latitude air masses is negligible.

7 Summary and conclusions

We presented high resolution cross-sections of CFC-11, O₃, and ClONO₂ measured by CRISTA-NF in the polar UTLS on 2 March 2010. The observations include vortex air masses, indicating the bottom edge of the polar vortex at ≈ 15.5 km. Two filaments with very low CFC-11 VMRs were observed that could be analysed in terms of transport and mixing. By means of ozone-CFC-11-relations one of these filaments could clearly be identified as a vortex filament, whereas the other filament has the same characteristics as air outside the vortex. Large parts of the trace gas fields and small-scale structures observed by CRISTA-NF can be quantitatively reproduced by CLaMS simulations. This confirms the excellent representation of advection and mixing in this model. Some small differences between the observations and simulations concern the ozone chemistry inside the polar vortex. Simulated ozone VMRs inside the vortex suggest a somewhat smaller ozone loss than observed values (up to 0.4 ppmv). Comparisons with satellite observations suggest that this deviation is mainly caused by an underestimation of the chlorine activation from the reservoir species HCl in the model.

Furthermore, we analysed the origin of the observed air masses based on a passive tracer concept. Each of these passive tracers represents another type of air mass (e.g. vortex, low-latitudes). An initialisation of the passive tracers on 15 January 2010 provides a picture that is consistent with the CRISTA-NF observations and even provides information on the origin of air masses that goes beyond the observation. Based on this scheme, we can show that several filaments had tropical origin and were transported towards the pole. A distinctive feature of the Arctic winter 2009/2010 was a sudden stratospheric warming in early December that led to a vortex split. As a consequence, a passive tracer experiment, initialised on 1 December 2009, fails to explain the CRISTA-NF observations made on 2 March 2010. But the comparison of the results of both passive tracer experiments (initialised on 1 December 2009 and 15 January 2010) provides information on the amount (about 45 %) of the contribution of high- and mid-latitude air masses to the re-established vortex at end of December 2009.

Title Page

Abstract

Introduction

Conclusions

References

Tables

Figures



Back

Close

Full Screen / Esc

Printer-friendly Version

Interactive Discussion



Acknowledgements. The RECONCILE project is funded under the European Commission Seventh Framework Programme (FP7) under the Grant number RECONCILE-226365-FP7-ENV-2008-1. We thank the RECONCILE Coordination and flight planning teams, MDB and Enviscope for the successful implementation of and support during the Arctic field campaign. The ECMWF data are provided by the European Center for Medium range Weather Forecast. We further thank W. Woiwode and H. Oelhaf from the Karlsruhe Institute of Technology (KIT) for providing the MIPAS-STR AHRs attitude measurements. Furthermore, we thank the AURA-MLS team, the MIPAS-ENV team, and the ACE-FTS team for providing data used for the initialisation of CLaMS.

References

- Bernath, P. F., McElroy, C. T., Abrams, M. C., Boone, C. D., Butler, M., Camy-Peyret, C., Carleer, M., Clerbaux, C., Coheur, P.-F., Colin, R., DeCola, P., DeMazière, M., Drummond, J. R., Dufour, D., Evans, W. F. J., Fast, H., Fussen, D., Gilbert, K., Jennings, D. E., Llewellyn, E. J., Lowe, R. P., Mahieu, E., McConnell, J. C., McHugh, M., McLeod, S. D., Michaud, R., Midwinter, C., Nassar, R., Nichitiu, F., Nowlan, C., Rinsland, C. P., Rochon, Y. J., Rowlands, N., Semeniuk, K., Simon, P., Skelton, R., Sloan, J. J., Soucy, M.-A., Strong, K., Tremblay, P., Turnbull, D., Walker, K. A., Walkty, I., Wardle, D. A., Wehrle, V., Zander, R., and Zou, J.: Atmospheric Chemistry Experiment (ACE): mission overview, *Geophys. Res. Lett.*, 32, L15S01, doi:10.1029/2005GL022386, 2005. 10469
- Dörnbrack, A., Pitts, M. C., Poole, L. R., Orsolini, Y. J., Nishii, K., and Nakamura, H.: The 2009–2010 Arctic stratospheric winter – general evolution, mountain waves and predictability of an operational weather forecast model, *Atmos. Chem. Phys.*, 12, 3659–3675, doi:10.5194/acp-12-3659-2012, 2012. 10478
- Douglass, A. R., Schoeberl, M. R., Stolarski, R. S., Waters III, J. J. M. R., Roche, A. E., and Massie, S. T.: Interhemispheric differences in springtime production of HCl and ClONO₂ in the polar vortices, *J. Geophys. Res.*, 100, 13967–13978, 1995. 10474
- Fastie, W.: Ebert Spectrometer Reflections, *Phys. Today*, 4, 37–43, 1991. 10467
- Fischer, H., Birk, M., Blom, C., Carli, B., Carlotti, M., von Clarmann, T., Delbouille, L., Dudhia, A., Ehnhalt, D., Endemann, M., Flaud, J. M., Gessner, R., Kleinert, A., Koopman, R., Langen, J., López-Puertas, M., Mosner, P., Nett, H., Oelhaf, H., Perron, G., Remedios, J.,

Small-scale transport structures in the Arctic winter 2009/2010

C. Kalicinsky et al.

Title Page

Abstract

Introduction

Conclusions

References

Tables

Figures



Back

Close

Full Screen / Esc

Printer-friendly Version

Interactive Discussion



**Small-scale
transport structures
in the Arctic winter
2009/2010**

C. Kalicinsky et al.

Title Page

Abstract

Introduction

Conclusions

References

Tables

Figures

◀

▶

◀

▶

Back

Close

Full Screen / Esc

Printer-friendly Version

Interactive Discussion

- Ridolfi, M., Stiller, G., and Zander, R.: MIPAS: an instrument for atmospheric and climate research, *Atmos. Chem. Phys.*, 8, 2151–2188, doi:10.5194/acp-8-2151-2008, 2008. 10469
- Grooß, J.-U., Günther, G., Müller, R., Konopka, P., Bausch, S., Schlager, H., Voigt, C., Volk, C. M., and Toon, G. C.: Simulation of denitrification and ozone loss for the Arctic winter 2002/2003, *Atmos. Chem. Phys.*, 5, 1437–1448, doi:10.5194/acp-5-1437-2005, 2005. 10469, 10489
- Grossmann, K. U., Offermann, D., Gusev, O., Oberheide, J., Riese, M., and Spang, R.: The CRISTA-2 mission, *J. Geophys. Res.*, 107, 8173, doi:10.1029/2001JD000667, 2002. 10465
- Günther, G., Müller, R., von Hobe, M., Stroh, F., Konopka, P., and Volk, C. M.: Quantification of transport across the boundary of the lower stratospheric vortex during Arctic winter 2002/2003, *Atmos. Chem. Phys.*, 8, 3655–3670, doi:10.5194/acp-8-3655-2008, 2008. 10466, 10469
- Hoffmann, L. and Alexander, M. J.: Retrieval of stratospheric temperatures from Atmospheric Infrared Sounder radiance measurements for gravity wave studies, *J. Geophys. Res.*, 114, D07105, doi:10.1029/2008JD011241, 2009. 10468
- Hoffmann, L., Kaufmann, M., Spang, R., Müller, R., Remedios, J. J., Moore, D. P., Volk, C. M., von Clarmann, T., and Riese, M.: Envisat MIPAS measurements of CFC-11: retrieval, validation, and climatology, *Atmos. Chem. Phys.*, 8, 3671–3688, doi:10.5194/acp-8-3671-2008, 2008. 10468
- Hoffmann, L., Weigel, K., Spang, R., Schroeder, S., Arndt, K., Lehmann, C., Kaufmann, M., Ern, M., Preusse, P., Stroh, F., and Riese, M.: CRISTA-NF measurements of water vapor during the SCOUT-O₃ Tropical Aircraft Campaign, *Adv. Space Res.*, 43, 74–81, doi:10.1016/j.asr.2008.03.018, 2009. 10466
- Hoor, P., Fischer, H., Lange, L., Lelieveld, J., and Brunner, D.: Seasonal variations of a mixing layer in the lowermost stratosphere as identified by the CO-O₃ correlation from in situ measurements, *J. Geophys. Res.*, 107, 4044, doi:10.1029/2000JD000289, 2002. 10465
- IPCC: Climate Change 2007: The Physical Science Basis, Contributions of Working Group I to the Fourth Assessment Report of the Intergovernmental Panel on Climate Change, edited by: Solomon, S., Qin, D., Manning, M., Chen, Z., Marquis, M., Averyt, K. B., Tignor, M., and Miller, H. L., Cambridge University Press, Cambridge, United Kingdom and New York, NY, USA, 2007. 10465
- Konopka, P., Steinhorst, H.-M., Grooß, J.-U., Günther, G., Müller, R., Elkins, J. W., Jost, H.-J., Richard, E., Schmidt, U., Toon, G., and McKenna, D. S.: Mixing and ozone loss in the 1999–

Small-scale transport structures in the Arctic winter 2009/2010

C. Kalicinsky et al.

[Title Page](#)
[Abstract](#)
[Introduction](#)
[Conclusions](#)
[References](#)
[Tables](#)
[Figures](#)
[⏪](#)
[⏩](#)
[◀](#)
[▶](#)
[Back](#)
[Close](#)
[Full Screen / Esc](#)
[Printer-friendly Version](#)
[Interactive Discussion](#)


2000 Arctic vortex: simulations with the three-dimensional Chemical Lagrangian Model of the Stratosphere (CLaMS), *J. Geophys. Res.*, 109, D02315, doi:10.1029/2003JD003792, 2004. 10465, 10468, 10469

5 Konopka, P., Günther, G., Müller, R., dos Santos, F. H. S., Schiller, C., Ravegnani, F., Ulanovsky, A., Schlager, H., Volk, C. M., Viciani, S., Pan, L. L., McKenna, D.-S., and Riese, M.: Contribution of mixing to upward transport across the tropical tropopause layer (TTL), *Atmos. Chem. Phys.*, 7, 3285–3308, doi:10.5194/acp-7-3285-2007, 2007. 10468

10 Kullmann, A., Riese, M., Olschewski, F., Stroh, F., and Grossmann, K. U.: Cryogenic infrared spectrometers and telescopes for the atmosphere – new Frontiers, *Proc. SPIE*, 5570, 423–432, 2004. 10467

Lait, L. R.: An alternative form for potential vorticity, *J. Atmos. Sci.*, 51, 1754–1759, 1994. 10470

15 McKenna, D. S., Grooß, J.-U., Günther, G., Konopka, P., Müller, R., Carver, G., and Sasano, Y.: A new Chemical Lagrangian Model of the Stratosphere (CLaMS) 2. formulation of chemistry scheme and initialization, *J. Geophys. Res.*, 107, 4256, doi:10.1029/2000JD000113, 2002a. 10466, 10469

20 McKenna, D. S., Konopka, P., Grooß, J.-U., Günther, G., Müller, R., Spang, R., Offermann, D., and Orsolini, Y.: A new Chemical Lagrangian Model of the Stratosphere (CLaMS) 1. formulation of advection and mixing, *J. Geophys. Res.*, 107, 4309, doi:10.1029/2000JD000114, 2002b. 10466, 10468, 10469

25 Müller, R. and Günther, G.: A generalized form of Lait's Modified Potential Vorticity, *J. Atmos. Sci.*, 60, 2229–2237, 2003. 10470, 10471

Müller, R., Tilmes, S., Konopka, P., Grooß, J.-U., and Jost, H.-J.: Impact of mixing and chemical change on ozone-tracer relations in the polar vortex, *Atmos. Chem. Phys.*, 5, 3139–3151, doi:10.5194/acp-5-3139-2005, 2005. 10475

30 Nash, E. R., Newman, P. A., Rosenfield, J. E., and Schoeberl, M. R.: An objective determination of the polar vortex using Ertel's potential vorticity, *J. Geophys. Res.*, 101, 9471–9478, 1996. 10470

Offermann, D., Grossmann, K.-U., Barthol, P., Knieling, P., Riese, M., and Trant, R.: Cryogenic Infrared Spectrometers and Telescopes for the Atmosphere (CRISTA) experiment and middle atmosphere variability, *J. Geophys. Res.*, 104, 16311–16325, doi:10.1029/1998JD100047, 1999. 10465

Plumb, R. A.: Tracer interrelationships in the stratosphere, *Rev. Geophys.*, 45, RG4005, doi:10.1029/2005RG000179, 2007. 10475

Small-scale transport structures in the Arctic winter 2009/2010

C. Kalicinsky et al.

[Title Page](#)
[Abstract](#)
[Introduction](#)
[Conclusions](#)
[References](#)
[Tables](#)
[Figures](#)
[⏪](#)
[⏩](#)
[◀](#)
[▶](#)
[Back](#)
[Close](#)
[Full Screen / Esc](#)
[Printer-friendly Version](#)
[Interactive Discussion](#)

- Riese, M., Tie, X., Brasseur, G., and Offermann, D.: Three-dimensional simulation of stratospheric trace gas distributions measured by CRISTA, *J. Geophys. Res.*, 104, 16419–16435, doi:10.1029/1999JD900178, 1999. 10465
- 5 Riese, M., Manney, G. L., Oberheide, J., Tie, X., Spang, R., and Küll, V.: Stratospheric transport by planetary wave mixing as observed during CRISTA-2, *J. Geophys. Res.*, 107, 8179, doi:10.1029/2001JD000629, 2002. 10465
- Riese, M., Ploeger, F., Rap, A., Vogel, B., Konopka, P., Dameris, M., and Forster, P.: Impact of uncertainties in atmospheric mixing on simulated UTLS composition and related radiative effects, *J. Geophys. Res.*, 117, D16305, doi:10.1029/2012JD017751, 2012. 10465
- 10 Santee, M., MacKenzie, I., Manney, G., Chipperfield, M., Bernath, P., Walker, K., Boone, C., Froidevaux, L., Livesey, N., and Waters, J.: A study of stratospheric chlorine partitioning based on new satellite measurements and modeling, *J. Geophys. Res.*, 113, D12307, doi:10.1029/2007JD009057, 2008. 10474
- Schroeder, S., Kullman, A., Preusse, P., Stroh, F., Weigel, K., Ern, M., Knieling, P., Olschewski, F., Spang, R., and Riese, M.: Radiance calibration of CRISTA-NF, *Adv. Space Res.*, 43, 1910–1917, doi:10.1016/j.asr.2009.03.009, 2009. 10467
- 15 Spang, R., Hoffmann, L., Kullmann, A., Olschewski, F., Preusse, P., Knieling, P., Schroeder, S., Stroh, F., Weigel, K., and Riese, M.: High resolution limb observations of clouds by the CRISTA-NF experiment during the SCOUT-O3 tropical aircraft campaign, *Adv. Space Res.*, 42, 1765–1775, doi:10.1016/j.asr.2007.09.036, 2008. 10466, 10467, 10471
- 20 Ungermann, J.: Improving retrieval quality for airborne limb sounders by horizontal regularisation, *Atmos. Meas. Tech.*, 6, 15–32, doi:10.5194/amt-6-15-2013, 2013. 10468
- Ungermann, J., Hoffmann, L., Preusse, P., Kaufmann, M., and Riese, M.: Tomographic retrieval approach for mesoscale gravity wave observations by the PREMIER Infrared Limb-Sounder, *Atmos. Meas. Tech.*, 3, 339–354, doi:10.5194/amt-3-339-2010, 2010. 10467
- 25 Ungermann, J., Kalicinsky, C., Olschewski, F., Knieling, P., Hoffmann, L., Blank, J., Woitode, W., Oelhaf, H., Hösen, E., Volk, C. M., Ulanovsky, A., Ravegnani, F., Weigel, K., Stroh, F., and Riese, M.: CRISTA-NF measurements with unprecedented vertical resolution during the RECONCILE aircraft campaign, *Atmos. Meas. Tech.*, 5, 1173–1191, doi:10.5194/amt-5-1173-2012, 2012. 10465, 10466, 10467, 10468, 10473
- 30 Ungermann, J., Pan, L. L., Kalicinsky, C., Olschewski, F., Knieling, P., Blank, J., Weigel, K., Guggenmoser, T., Stroh, F., Hoffmann, L., and Riese, M.: Filamentary structure in chemical

Small-scale transport structures in the Arctic winter 2009/2010

C. Kalicinsky et al.

[Title Page](#)
[Abstract](#)
[Introduction](#)
[Conclusions](#)
[References](#)
[Tables](#)
[Figures](#)




[Back](#)
[Close](#)
[Full Screen / Esc](#)
[Printer-friendly Version](#)
[Interactive Discussion](#)

tracer distributions near the subtropical jet following a wave breaking event, *Atmos. Chem. Phys. Discuss.*, 13, 5039–5089, doi:10.5194/acpd-13-5039-2013, 2013. 10467

von Hobe, M., Bekki, S., Borrmann, S., Cairo, F., D'Amato, F., Di Donfrancesco, G., Dörnbrack, A., Ebersoldt, A., Ebert, M., Emde, C., Engel, I., Ern, M., Frey, W., Griessbach, S., Grooß, J.-U., Gulde, T., Günther, G., Hösen, E., Hoffmann, L., Homonnai, V., Hoyle, C. R., Isaksen, I. S. A., Jackson, D. R., Jánosi, I. M., Kandler, K., Kalicinsky, C., Keil, A., Khaykin, S. M., Khosrawi, F., Kivi, R., Kuttippurath, J., Laube, J. C., Lefèvre, F., Lehmann, R., Ludmann, S., Luo, B. P., Marchand, M., Meyer, J., Mitev, V., Molleker, S., Müller, R., Oelhaf, H., Olschewski, F., Orsolini, Y., Peter, T., Pfeilsticker, K., Piesch, C., Pitts, M. C., Poole, L. R., Pope, F. D., Ravegnani, F., Rex, M., Riese, M., Röckmann, T., Rognerud, B., Roiger, A., Rolf, C., Santee, M. L., Scheibe, M., Schiller, C., Schlager, H., Siciliani de Cumis, M., Sitnikov, N., Søvde, O. A., Spang, R., Spelten, N., Stordal, F., Sumińska-Ebersoldt, O., Viciani, S., Volk, C. M., vom Scheidt, M., Ulanovski, A., von der Gathen, P., Walker, K., Wegner, T., Weigel, R., Weinbuch, S., Wetzels, G., Wienhold, F. G., Wintel, J., Wohltmann, I., Woiwode, W., Young, I. A. K., Yushkov, V., Zobrist, B., and Stroh, F.: Reconciliation of essential process parameters for an enhanced predictability of Arctic stratospheric ozone loss and its climate interactions, *Atmos. Chem. Phys. Discuss.*, 12, 30661–30754, doi:10.5194/acpd-12-30661-2012, 2012. 10466, 10478

Waters, J., Froidevaux, L., Harwood, R., Jarnot, R., Pickett, H., Read, W., Siegel, P., Cofield, R., Filipiak, M., Flower, D., Holden, J., Lau, G., Livesey, N., Manney, G., Pumphrey, H., Santee, M., Wu, D., Cuddy, D., Lay, R., Loo, M., Perun, V., Schwartz, M., Stek, P., Thurstans, R., Boyles, M., Chandra, K., Chavez, M., Chen, G.-S., Chudasama, B., Dodge, R., Fuller, R., Girard, M., Jiang, J., Jiang, Y., Knosp, B., LaBelle, R., Lam, J., Lee, K., Miller, D., Oswald, J., Patel, N., Pukala, D., Quintero, O., Scaff, D., Van Snyder, W., Tope, M., Wagner, P., and Walch, M.: The Earth Observing System Microwave Limb Sounder (EOS MLS) on the Aura Satellite, *IEEE T. Geosci. Remote*, 44, 1075–1092, doi:10.1109/TGRS.2006.873771, 2006. 10469

Weigel, K., Riese, M., Hoffmann, L., Hofer, S., Kalicinsky, C., Knieling, P., Olschewski, F., Preusse, P., Spang, R., Stroh, F., and Volk, C. M.: CRISTA-NF measurements during the AMMA-SCOUT-O3 aircraft campaign, *Atmos. Meas. Tech.*, 3, 1437–1455, doi:10.5194/amt-3-1437-2010, 2010. 10468

Weigel, K., Hoffmann, L., Günther, G., Khosrawi, F., Olschewski, F., Preusse, P., Spang, R., Stroh, F., and Riese, M.: A stratospheric intrusion at the subtropical jet over the Mediter-

ranean Sea: air-borne remote sensing observations and model results, Atmos. Chem. Phys., 12, 8423–8438, doi:10.5194/acp-12-8423-2012, 2012. 10466, 10468
WMO: Scientific Assessment of Ozone Depletion: 2006, Global Ozone Research and Monitoring Project – Report No. 50, Geneva, Switzerland, 2007. 10472

Small-scale transport structures in the Arctic winter 2009/2010

C. Kalicinsky et al.

Title Page

Abstract

Introduction

Conclusions

References

Tables

Figures



Back

Close

Full Screen / Esc

Printer-friendly Version

Interactive Discussion

Small-scale transport structures in the Arctic winter 2009/2010

C. Kalicinsky et al.

Table 1. Integrated micro windows (IMW) as used in the retrieval and the corresponding main retrieval targets.

IMW #	spectral range (cm ⁻¹)	main target
1	777.5–778.5	O ₃
2	784.0–785.0	H ₂ O
3	787.0–790.0	offset
4	791.5–793.0	temperature
5	794.1–795.0	PAN
6	795.5–796.5	O ₃
7	796.6–797.5	CCl ₄
8	808.0–809.0	HCFC-22
9	810.0–813.0	ClONO ₂
10	820.5–821.5	HCFC-22
11	831.0–832.0	aerosol
12	846.0–847.0	CFC-11
13	863.0–866.0	HNO ₃

[Title Page](#)
[Abstract](#)
[Introduction](#)
[Conclusions](#)
[References](#)
[Tables](#)
[Figures](#)
[◀](#)
[▶](#)
[◀](#)
[▶](#)
[Back](#)
[Close](#)
[Full Screen / Esc](#)
[Printer-friendly Version](#)
[Interactive Discussion](#)

Small-scale transport structures in the Arctic winter 2009/2010

C. Kalicinsky et al.

[Title Page](#)[Abstract](#)[Introduction](#)[Conclusions](#)[References](#)[Tables](#)[Figures](#)[⏪](#)[⏩](#)[◀](#)[▶](#)[Back](#)[Close](#)[Full Screen / Esc](#)[Printer-friendly Version](#)[Interactive Discussion](#)**Table 2.** Summary of the CLaMS setup.

horizontal resolution (mean distance of air parcels)	70 km
horizontal range	0°–90° N
vertical levels	50
vertical resolution	≈ 500 m (for $\zeta > 380$ K)
vertical range	300 K > ζ < 900 K
meteorological wind fields	ECMWF ERA interim data (1° × 1°)
heating/cooling rates	ECMWF clear sky radiative heating rate
time step Δt	24 h
Lyapunov exponent λ_c	1.5 d ⁻¹
NAT nucleation rate	8 · 10 ⁻⁵ cm ⁻¹ h ⁻¹
	(10 times larger as in Groß et al., 2005)

Small-scale transport structures in the Arctic winter 2009/2010

C. Kalicinsky et al.

Title Page

Abstract

Introduction

Conclusions

References

Tables

Figures

◀

▶

◀

▶

Back

Close

Full Screen / Esc

Printer-friendly Version

Interactive Discussion

Table 3. Summary of the modified potential vorticity boundaries for the artificial tracers and the corresponding type of air masses.

mPV boundary (in PVU)	type of air masses
0–8	low-latitude
8–14.7	mid-latitude
14.7–19.8	high-latitude
> 19.8	vortex

Small-scale transport structures in the Arctic winter 2009/2010

C. Kalicinsky et al.

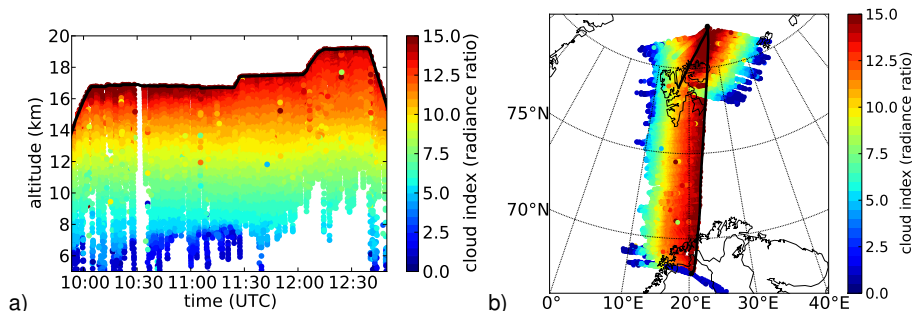


Fig. 1. CRISTA-NF cloud index during RECONCILE flight 11 (2 March 2010) as cross-section plot (a) and in longitude latitude domain (b). The solid black line shows the observer altitude in the cross-section plot and the observer location otherwise. The turn of the aircraft is indicated by the white vertical stripe in the cross-section plot due to the lack of measurements during the turn.

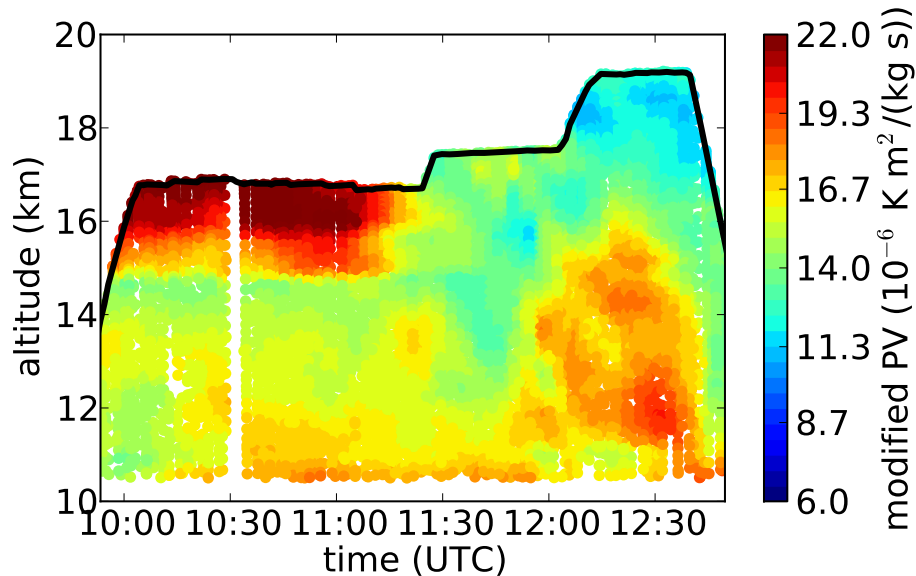


Fig. 2. Modified potential vorticity derived from ECMWF data at the tangent points of the CRISTA-NF measurements during RECONCILE flight 11 (2 March 2010). Details see caption of Fig. 1.

Small-scale transport structures in the Arctic winter 2009/2010

C. Kalicinsky et al.

Title Page	
Abstract	Introduction
Conclusions	References
Tables	Figures
⏪	⏩
◀	▶
Back	Close
Full Screen / Esc	
Printer-friendly Version	
Interactive Discussion	



Small-scale transport structures in the Arctic winter 2009/2010

C. Kalicinsky et al.

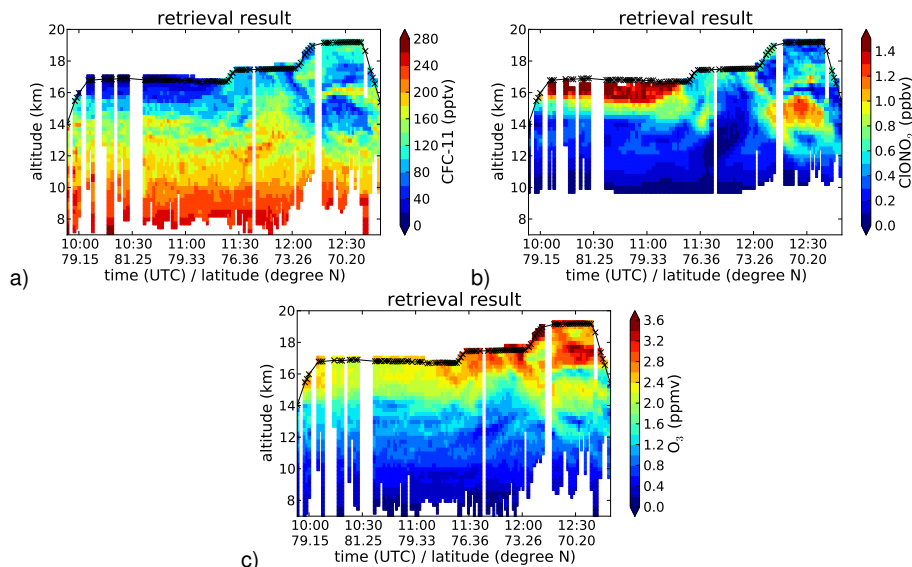


Fig. 3. CRISTA-NF retrieval results for CFC-11, ClONO_2 , and O_3 for RECONCILE flight 11 (2 March 2010). All results with a measurement contribution less than 0.7 are excluded. The solid black line shows the observer altitude and the position (time) of each profile is marked by a black cross. Additionally, the abscissa displays the latitude at 12 km tangent height. Results are shown between flight altitude and the lowest tangent height of a valid measurement in the corresponding profile. The vertical white stripes show times with insufficient measurements by CRISTA-NF caused due to strong aircraft movements (e.g. turn at about 10:30 UTC).

Title Page

Abstract

Introduction

Conclusions

References

Tables

Figures

◀

▶

◀

▶

Back

Close

Full Screen / Esc

Printer-friendly Version

Interactive Discussion

Small-scale
transport structures
in the Arctic winter
2009/2010

C. Kalicinsky et al.

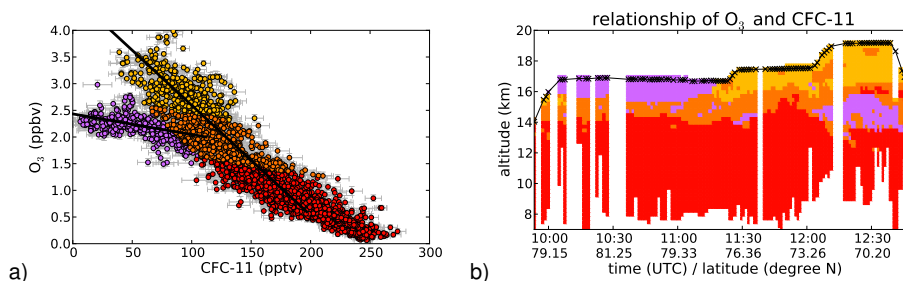


Fig. 4. Relationship between CFC-11 and O₃ for retrieved trace gas VMRs. Panel (a) shows a scatter plot for all measured air parcels with two black lines corresponding to typical relationships for vortex and non-vortex air. Purple parcels are thus categorised as vortex air, while yellow and red parcels consist of non-vortex air. Orange parcels cannot be clearly distinguished according to this criterion. The error bars show the precision of the measurements. Panel (b) shows the geo-spatial distribution of the same air parcels using the same colours.

Small-scale transport structures in the Arctic winter 2009/2010

C. Kalicinsky et al.

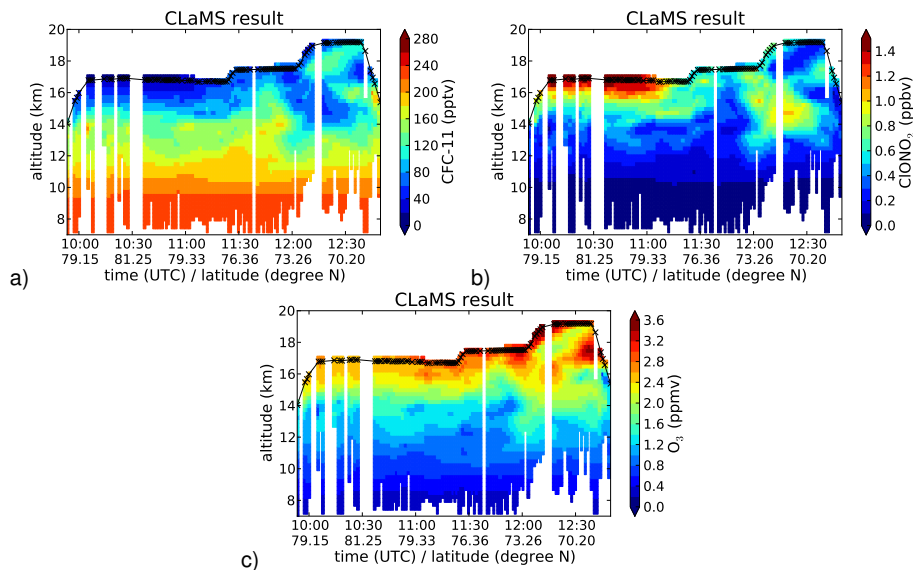


Fig. 5. CLaMS results for CFC-11, ClONO₂, and O₃ for RECONCILE flight 11 (2 March 2010). Details see caption of Fig. 3.

[Title Page](#)
[Abstract](#)
[Introduction](#)
[Conclusions](#)
[References](#)
[Tables](#)
[Figures](#)
[⏪](#)
[⏩](#)
[◀](#)
[▶](#)
[Back](#)
[Close](#)
[Full Screen / Esc](#)
[Printer-friendly Version](#)
[Interactive Discussion](#)

Small-scale
transport structures
in the Arctic winter
2009/2010

C. Kalicinsky et al.

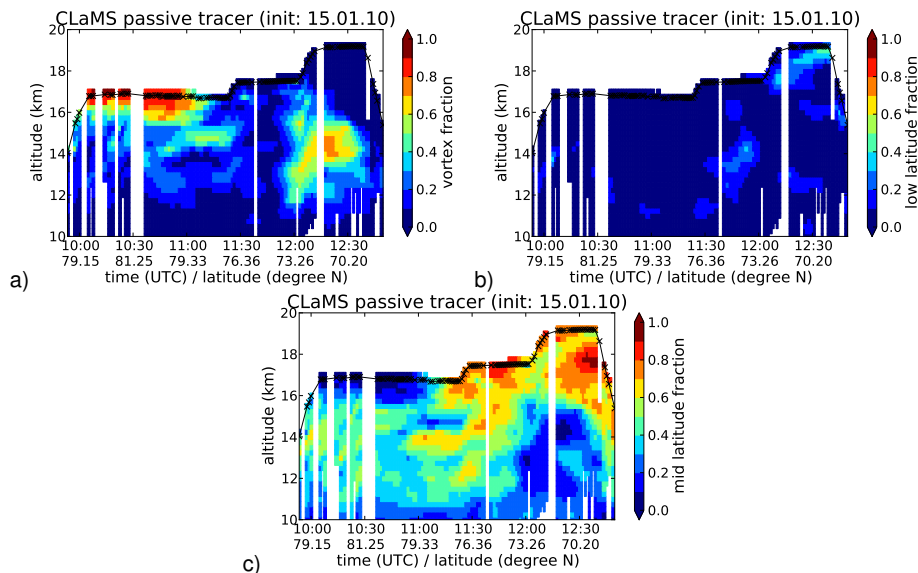


Fig. 6. Cross-section of the CLaMS vortex tracer, low-latitude tracer, and mid-latitude tracer with initialisation on 15 January. Details see caption of Fig. 3.

Small-scale transport structures in the Arctic winter 2009/2010

C. Kalicinsky et al.

Title Page

Abstract

Introduction

Conclusions

References

Tables

Figures

⏪

⏩

◀

▶

Back

Close

Full Screen / Esc

Printer-friendly Version

Interactive Discussion

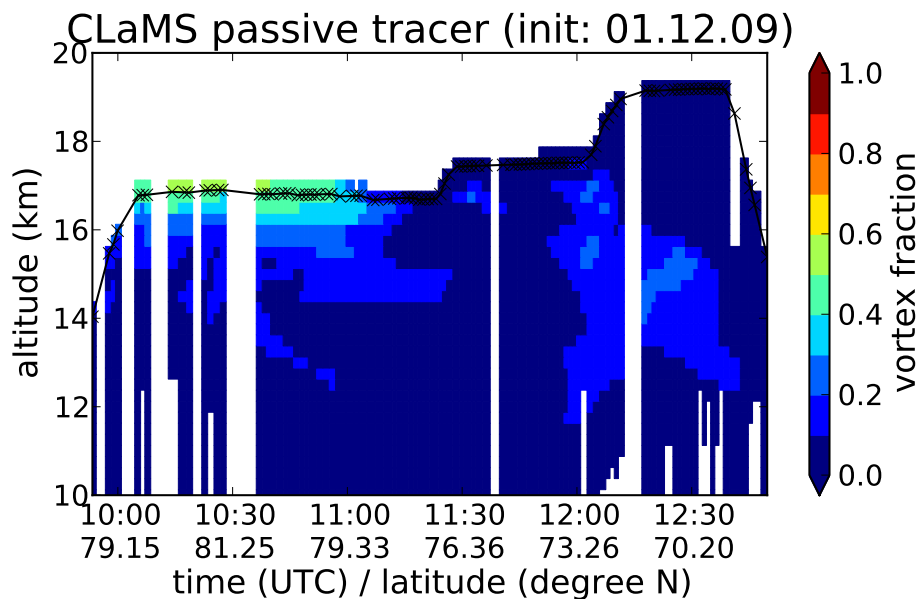


Fig. 7. Cross-section of the CLaMS vortex tracer with initialisation on 1 December. Details see caption of Fig. 3.

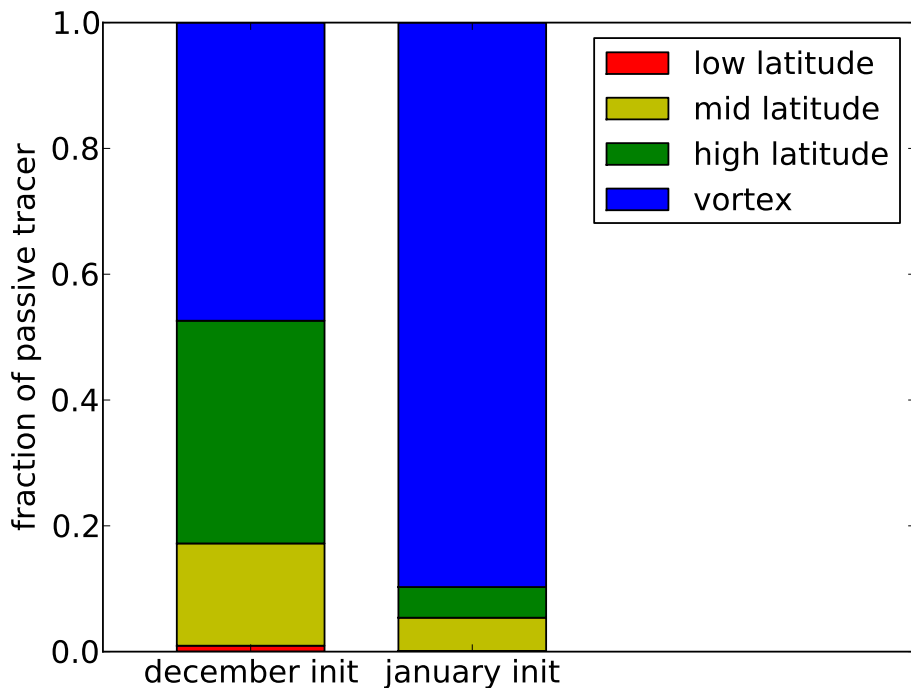


Fig. 8. Fraction of passive tracers for low-latitude, mid-latitude, high-latitude and vortex air masses inside the polar vortex (10:05 to 11:00 UTC) around flight altitude (≈ 450 K potential temperature) for December and January initialisation.

Small-scale transport structures in the Arctic winter 2009/2010

C. Kalicinsky et al.

Title Page

Abstract Introduction

Conclusions References

Tables Figures

⏪ ⏩

⏴ ⏵

Back Close

Full Screen / Esc

Printer-friendly Version

Interactive Discussion

